Earth Planet. Sci. Lett. 632 (2024) 118642

Contents lists available at ScienceDirect

Earth and Planetary Science Letters

journal homepage: www.elsevier.com/locate/epsl

# A recipe for making potassium-rich magmas in collisional orogens: New insights from K and Fe isotopes

De-Hong Du [a], Xiang-Long Luo [a], Xiao-Lei Wang [a], Martin R. Palmer [b], E.Yalçın Ersoy [c], Weiqiang Li [a,*]

[a] State Key Laboratory for Mineral Deposits Research, School of Earth Sciences and Engineering, Nanjing University, Nanjing 210023, China
[b] School of Ocean and Earth Science, University of Southampton, Southampton SO14 3ZH, UK
[c] Dokuz Eylül Üniversitesi, Mühendislik Fakültesi, Jeoloji Mühendisliği Bölümü, TR-35160 Izmir, Türkiye

ARTICLE INFO

Editor: Dr R. Hickey-Vargas

*Key words:*
Ultrapotassic rocks
Collisional orogen
Fe isotopes
K isotopes
Western Anatolia

ABSTRACT

Ultrapotassic volcanism commonly occurs following calc-alkaline magmatism in continental collisional tectonic zones, but some key aspects of this transition remain ambiguous. In particular, there are uncertainties regarding the changing nature of the mantle source and the contribution of recycled continental material during the petrogenesis of ultrapotassic igneous rocks. Here, we show that the calc-alkaline to ultrapotassic transition in magmatism in Western Anatolia (Türkiye) during the past 55 Ma was associated with conspicuous shifts in the K and Fe isotope compositions of the bulk eruptive rocks. The ~52–17 Ma transitional (tholeiitic to calc-alkaline) and calc-alkaline rocks show low $\delta^{56}$Fe (0.05 ± 0.07 ‰, 1SD) and high $\delta^{41}$K values (from –0.41 ‰ to 0.00 ‰), relative to the overall higher $\delta^{56}$Fe (0.16 ± 0.05 ‰, 1SD) and lower $\delta^{41}$K values (from –0.32 ‰ to –0.55 ‰) of the ~19–15 Ma shoshonitic-ultrapotassic rocks in this area. The low $\delta^{41}$K values observed in the shoshonitic-ultrapotassic rocks are interpreted to reflect incorporation of potassium from deeply subducted recycled continental crust and the heavy Fe isotope signatures of these rocks imply a pyroxenite source. The rapid onset and short duration of eruption of the shoshonitic-ultrapotassic rocks is consistent with formation of phlogopite-pyroxenite veins within the peridotite mantle during slab rollback and/or breakoff. These veins were then rapidly and completely consumed by upwelling hot asthenospheric mantle.

## 1. Introduction

Collisional orogens are major sites for continental crust recycling and mantle-crust interaction and have played an important role in Earth's chemical evolution, but how recycled continental components remold the Earth's mantle remains unclear (e.g., Stern, 2002; Sobolev et al., 2007; Prelević et al., 2013). One way to detect the changing physical and chemical properties of the mantle beneath collisional zones is by studying mantle-derived magmas.

The enhanced magmatic activity during an orogeny typically starts with Andean-type, continental-arc, calc-alkaline magmatism, and is then followed by ultrapotassic magmatism. Relative to mid-ocean ridge basalts (~0.16 wt% $K_2O$; Gale et al., 2013), the continental collisional ultrapotassic lavas exhibit enhanced K enrichment (i.e., $K_2O$ >3 wt%, $K_2O/Na_2O$ >2, and MgO >3 wt%; Foley et al., 1987) compared to calc-alkaline rocks formed in continental arcs ($K_2O$ ≤3 wt% at MgO >3 wt%; Ersoy and Palmer, 2013). Hence, either the mantle beneath continental collision zones is more strongly contaminated by K compared to continental arc settings, and/or K is more effectively extracted from the contaminated mantle in collision zones in a manner that may reflect the mantle mineralogy.

Trace-element and radiogenic isotope signatures indicate greater involvement of subducted continental materials into the mantle source regions of ultrapotassic magmas relative to calc-alkaline magmas, and thus the K-rich magmas have been interpreted as the partial melts of metasomatized lithospheric mantle (e.g., Tommasini et al., 2011; Prelević et al., 2012; Ersoy and Palmer, 2013). However, the sources of K in ultrapotassic magmas and associated K-enrichment mechanism are still unclear. Furthermore, the nature of the metasomatized lithospheric mantle source of the ultrapotassic magmas remains uncertain, with two main competing lithologies proposed: (1) phlogopite-pyroxenite (e.g., Hirschmann et al., 2003; Prelević et al., 2012; Guo et al., 2015); and (2) phlogopite-peridotite (e.g., Mallik et al., 2015; Condamine et al., 2016; Xu et al., 2017a).

* Corresponding author.
*E-mail address:* liweiqiang@nju.edu.cn (W. Li).

https://doi.org/10.1016/j.epsl.2024.118642
Received 9 October 2023; Received in revised form 21 February 2024; Accepted 29 February 2024
Available online 5 March 2024

Potassium and iron are both major elements in calc-alkaline to ultrapotassic rocks. Interestingly, both exhibit stable isotope variations that can be used to constrain their sources and the lithological identities in collisional tectonic zones, respectively. Potassium isotopes exhibit little fractionation during mantle partial melting and mafic-intermediate magma differentiation (e.g., Tuller-Ross et al., 2019; Hu et al., 2021b). However, K isotopes can fractionate significantly during chemical weathering because heavy K isotopes are preferentially leached by waters, leaving the weathered residues enriched in light K isotopes (e.g., Li et al., 2019; Hu et al., 2020). In addition, extremely light K isotope signatures are observed in the exhumed eclogites, indicating that metamorphic dehydration processes also preferentially release heavy K isotopes into fluids (Liu et al., 2020). Therefore, magmas that have incorporated supracrustal material in their mantle sources may contain lighter K isotope compositions (e.g., Wang et al., 2021b; Hu et al., 2021a), while the incorporation of the slab-derived fluids into mantle sources can produce magmas with K isotope composition heavier than the primitive mantle (e.g., Liu et al., 2021; Hu et al., 2021a; Miao et al., 2023). Thus, K isotopes offer direct constraints on the sources of potassium in orogenic magmas.

Recent studies have shown that Fe isotopes can be used to distinguish lithological features of the sources of mantle-derived rocks (e.g., Williams and Bizmis, 2014; Konter et al., 2016; Wang et al., 2021a). Regardless of the origin of pyroxenites, including cumulate pyroxenites and secondary pyroxenites, Fe isotope compositions of pyroxene-rich xenoliths are systematically heavier than those of olivine-dominated peridotite with $\Delta^{56}Fe_{pyroxenite\text{-}peridotite}$ of ~0.1 ‰ (Johnson et al., 2020). In the former case pyroxenites are likely crystallized from

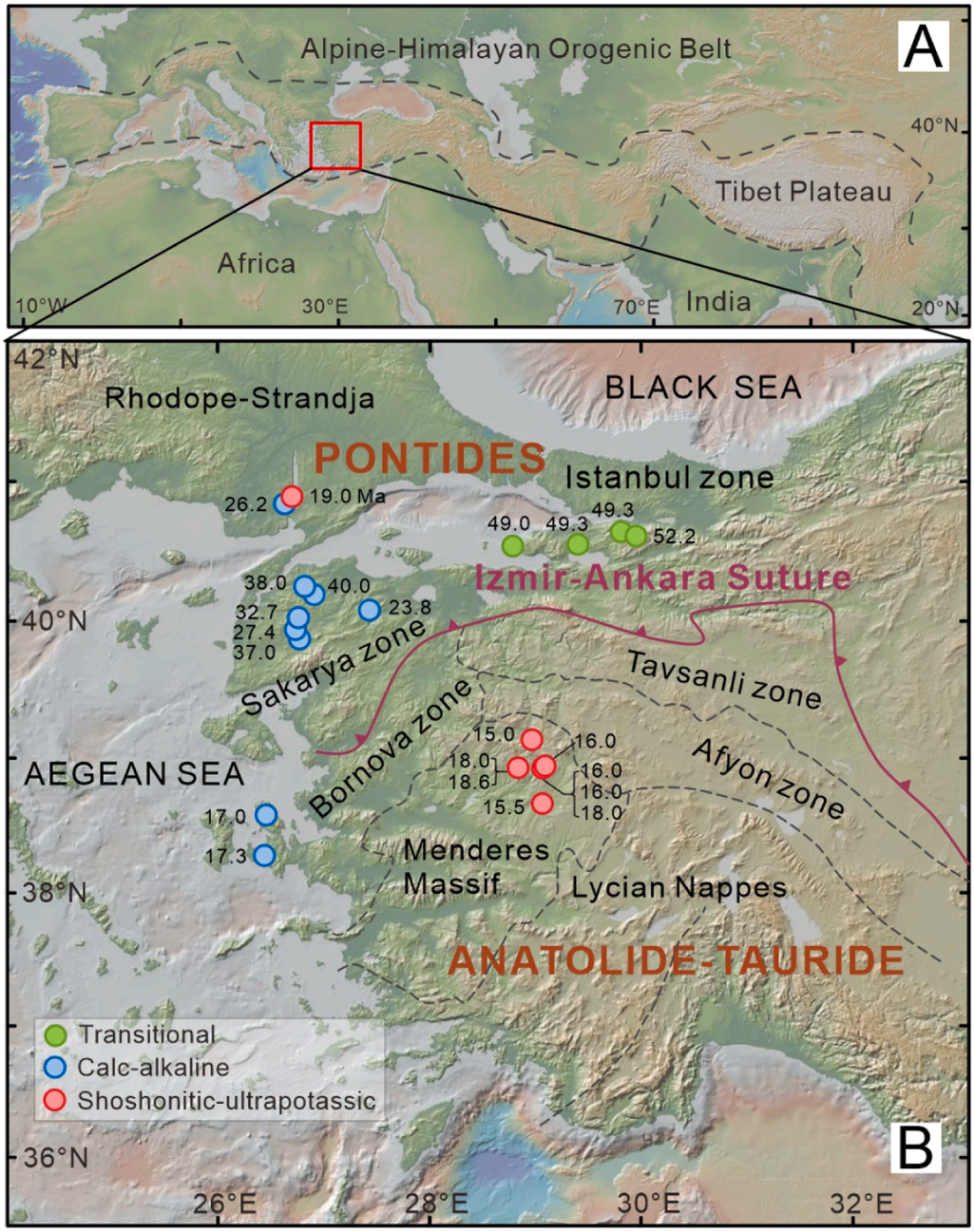


**Fig. 1.** (A) Overview map showing the Alpine-Himalayan Orogenic belt from Spain to Tibet. (B) Simplified geological map showing the main tectonic features of Western Anatolia, Türkiye (modified from Prelević et al., 2012). The black numbers represent the age of the investigated samples (Palmer et al., 2019). The base maps in (A) and (B) were generated using the GeoMapApp (http://www.geomapapp.org/).

evolved melts that are enriched in heavy Fe isotopes (Williams and Bizmis, 2014); in the latter they are interaction products between crust-derived melt and peridotite, likely obtaining heavy Fe isotope signatures by Fe-Mg inter-diffusion (Zhao et al., 2017; Su et al., 2015). Furthermore, crystal chemical studies indicate that $Fe^{3+}$-bearing pyroxenes have shorter and stiffer Fe-O bonds and thus tend to concentrate heavy Fe isotopes relative to $Fe^{3+}$-scarce olivine (Macris et al., 2015; Sossi and O'Neil, 2017). As partial melting of mantle sources preferentially consumes pyroxenes relative to olivine, the melts derived from a pyroxenitic source are thus expected to have heavier Fe isotope compositions than those from a peridotite mantle source (Williams and Bizmis, 2014). Thus, studies of Fe and K isotopes of the magmatic products of continental collision orogens can yield information concerning both the mineralogy of the mantle source and the involvement of recycled crustal material.

Western Anatolia (Türkiye) hosts a classic series of Eocene to Miocene volcanic rocks produced during collisional and post-collisional processes in the Late Cretaceous continental collision in the region. Collisional processes include southward migrating accretion of continental fragments from the Late Cretaceous in the north to the Eocene in the south. Hence, the magmatic products with geochemical signatures that range from calc-alkaline to ultrapotassic affinities can be considered as syn- to post-collisional volcanic series (Ersoy and Palmer, 2013; Palmer et al., 2019), and present an ideal setting to examine the utility of K and Fe isotope studies in elucidating the evolution of K sources and mantle composition during the geochemical evolution of orogenic volcanism.

## 2. Geological background and samples

Western Anatolia forms part of the Alpine-Himalayan orogenic belt (Fig. 1A), with magmatism in this region marking the closure of the northern Neotethys Ocean and subsequent continental collision and crustal accretion (e.g., Pourteau et al., 2016). Western Anatolia contains the Pontides with Laurasian affinity in the north and the Anatolides-Taurides with Gondwana affinity in the south. Collision between the two domains is marked by the Izmir-Ankara suture zone that formed during the Late Cretaceous to Paleocene (Fig. 1B; Moix et al., 2008). The Pontides domain likely represents a magmatic arc formed in response to the northward subduction of the Neotethys plate during the Late Cretaceous (e.g., Ersoy and Palmer, 2013). The Anatolides-Tauride domain comprises strongly metamorphosed Anatolides in the north and the unmetamorphosed Taurides further south. The northern Anatolides contain oceanic accretionary complexes which experienced amphibolite- and blueschist- facies metamorphism in the upper and lower sections, respectively (e.g., Pourteau et al., 2016). During the Eocene, N-S extension occurred in the northern part of the area (e.g., Rhodopes and Thrace Basins) during the post-collision stage, while the southern parts of the area were still undergoing crustal accretion in an ongoing compressional regime. Therefore, we use the term "syn-collisional" for the northern Eocene magmatic units. During the Oligocene to Miocene, there was further N-S extension throughout the region, and the Menderes Massif and westernmost Pontides were exhumed due to roll-back of the subducted African slab (Erkül and Erkül, 2012; Ersoy and Palmer, 2013).

Magmatism in Western Anatolia is characterized by the systematic younging from north to south in response to the southward lithospheric slab roll-back (e.g., Prelević et al., 2012; Ersoy and Palmer, 2013; Pourteau et al., 2016). The magmatic rocks have been systematically described and reviewed by Ersoy and Palmer (2013; and references therein) and are briefly summarized here. Their geochemistry changed from transitional (tholeiitic to calc-alkaline) to high-K calc-alkaline during Eocene to Oligocene (52–34 Ma) in the Pontides, which show arc-like geochemical signatures. Further to the south, Miocene magmatic activity is represented by high-K calc-alkaline and associated shoshonitic-ultrapotassic volcanism in the Anatolides-Taurides and was coeval with widespread ~E-W extension in this area. The magmatism ended with Na-alkaline basalts with OIB-like intraplate affinity that likely resulted from asthenospheric upwelling in the late Miocene to Holocene.

The volcanic rocks selected for K and Fe isotope analyses consist of 22 samples ranging from low-K calc-alkaline to shoshonitic-ultrapotassic series (Fig. 2A) that range in age from ~52 Ma to 15 Ma (Fig. 2B). These samples represent a magmatic series generated during the period from continental-continental collision to post-collisional extension (Ersoy and Palmer, 2013; Palmer et al., 2019). Major and trace elements, Sr, Nd, and B isotope data of these samples are presented in Palmer et al. (2019) and references therein. The samples can be divided into three types following the classification of Palmer et al. (2019): (1) Eocene (~52–49 Ma) tholeiitic to calc-alkaline type (referred to as the "transitional" type in the figures and later sections), (2) Eocene-Miocene (~43–16 Ma) calc-alkaline type, and (3) Miocene (~19–15 Ma) shoshonitic-ultrapotassic type. As shown in Fig. 2, the transitional samples are characterized by low contents of $K_2O$ (0.25–2.15 wt%), and low ratios of $K_2O/Na_2O$ (0.11–0.58) and La/Yb (1.9–7.0). The calc-alkaline samples show intermediate $K_2O$ contents (0.77–3.19 wt%), and intermediate ratios of $K_2O/Na_2O$ (0.24–0.95) and La/Yb (6.4–27). The shoshonitic-ultrapotassic samples show the highest $K_2O$ contents (2.73–8.83 wt%), and the highest ratios of $K_2O/Na_2O$ (0.75–4.14) and La/Yb (20.1–44.2). In addition, two gneisses, represented basement rocks, were selected for K and Fe isotope analysis.

## 3. Analytical methods

Analyses of whole-rock Fe and K isotope compositions were performed at the State Key Laboratory for Mineral Deposits Research, Nanjing University, China. For each sample, ~20 mg of bulk rock powder was digested in Teflon beakers using 4 ml 1:1 mixture of concentrated $HNO_3$–HF on a hotplate for two days. Next, the sample was dried on hotplate and re-dissolved in 2 ml 6 M HCl. 0.1 ml of the solution was taken and diluted to 10 ml and measured for major element (e.g., K, Mg, and Fe) concentrations on an Inductively Coupled Plasma Optical Emission Spectrometer (ICP-OES). An aliquot of the sample solution containing 100 μg of Fe was processed using ion-exchange column chemistry with a chloride-form AG MP-1 anion-exchange resin (100–200 mesh, 0.2 mL) for Fe purification following Du et al. (2017). Potassium was quantitatively eluted off the Fe column as the matrix, collected and dried in a new Teflon beaker, treated with concentrated $HNO_3$ and then dissolved in 1 ml 1.5 M $HNO_3$. An aliquot of the solution containing 50–100 μg K was processed using a two-stage ion exchange column procedure (Li et al., 2016). In the first step, the sample solution was loaded onto a column filled with 1 mL BioRad AG50W-X12 resin (100–200 mesh) to separate K from Na, Al, Ca, and Ti. The collected sample solution from the first step was then passed through a column containing 0.4 mL BioRad AG50W-X8 resin to separate K from Mg and other matrix elements. The recovery of K after column chemistry was >99 %.

The K isotope ratios were measured with a dry and hot plasma setting on the Nu 1700 Sapphire multi–collector–inductively coupled plasma–mass spectrometer (MC–ICP–MS). The analytical procedure and detailed conditions are similar to those of An et al. (2022). Sample solutions were introduced into the Ar plasma via an Aridus III desolvating nebulizer system at the RF power of 1300 W. The signals of $^{39}K^+$ and $^{41}K^+$ were collected simultaneously at the $^{40}Ar^1H^+$-free shoulder using high mass resolution mode (mass resolving power >16,000). The resulting signals were ~60 V of $^{39}K^+$ and ~5 V of $^{41}K^+$for solutions with 3 ppm K. Instrument mass bias was corrected by standard-sample-standard bracketing method. The isotope results are reported using the delta notion (δ):

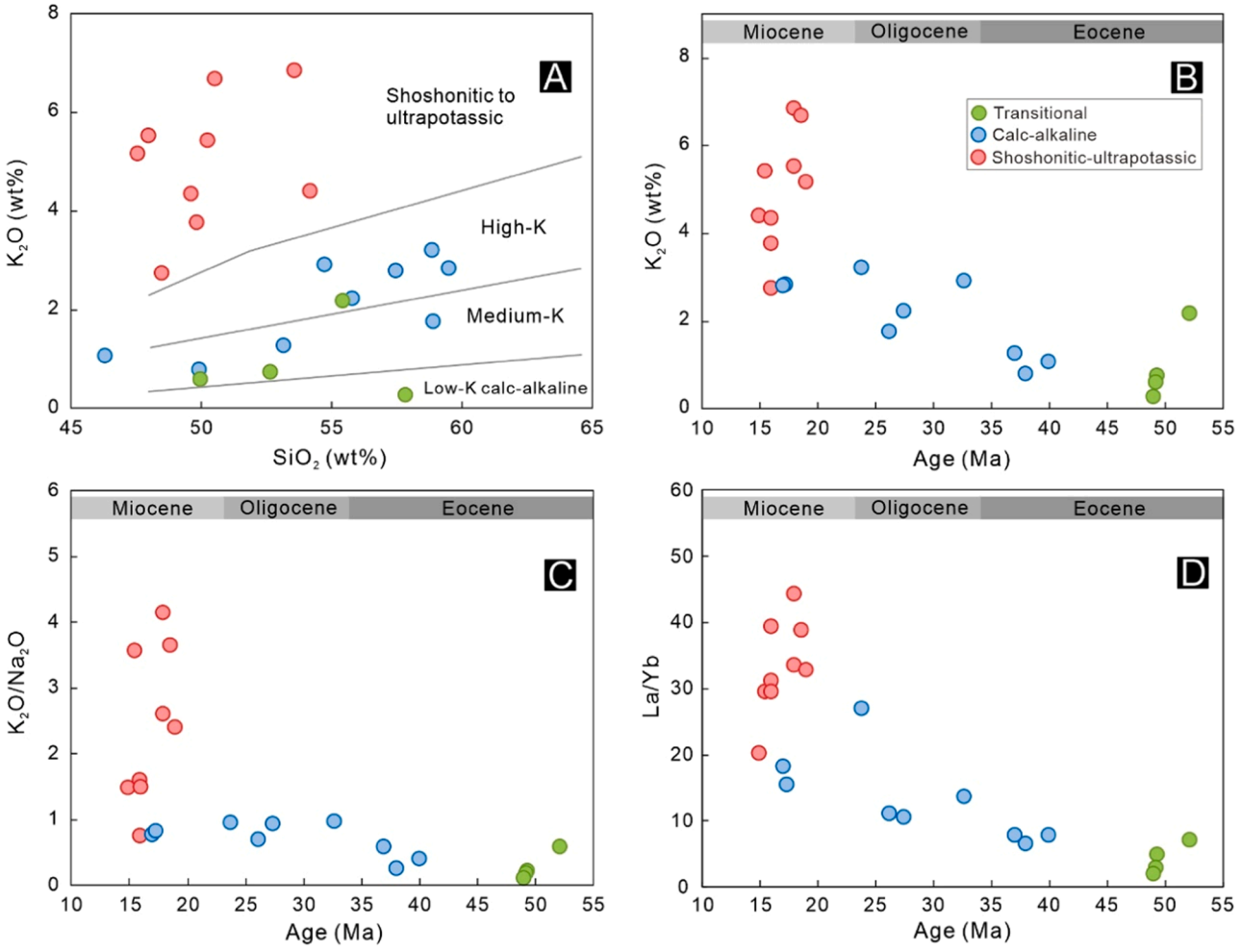


**Fig. 2.** Geochemical classification (A) and evolution (B-D) of Western Anatolian volcanic rocks. (A) $K_2O$ versus $SiO_2$ (wt%); (B) $K_2O$ (wt%) versus Age (Ma); (C) $K_2O$/$Na_2O$ versus Age (Ma); (C) La/Yb versus Age (Ma).

$$\delta^{41}K_{sample} = \left[\left(^{41}K/^{39}K\right)_{sample} \Big/ \left(^{41}K/^{39}K\right)_{NIST\ \ SRM\ \ 3141a} - 1\right] \times 1000\ [0/00]$$

The long-term external reproducibility of K isotope analyses of a pure K solution (purchased from SPEX Company, labeled as "A-K") over six months is ±0.07 ‰ (2SD) for $^{41}K/^{39}K$ (An et al., 2022). The K isotope compositions of the purified geochemical standards that were analyzed with the samples of this study, BCR-2 ($\delta^{41}K = -0.51 \pm 0.07$‰; $n = 3$, 2SD), BHVO-2 ($\delta^{41}K = -0.36 \pm 0.08$‰; $n = 6$, 2SD) and seawater ($\delta^{41}K = 0.07 \pm 0.09$‰; $n = 4$, 2SD), are all consistent within error with previously published results (e.g., Wang and Jacobsen, 2016; Ku and Jacobsen, 2020; Moynier et al., 2021).

Fe isotope analysis was performed on a Nu 1700 Sapphire MC-ICP-MS in wet-plasma mode with a mass resolving power of ~8000 under moderate resolution setting. The interference of $^{40}Ar^{16}O^+$ on $^{56}Fe^+$ were fully resolved using the medium resolution setting of the instrument. The resulting sensitivity was ~6 V/ppm for $^{56}Fe$, with a 3 ppm Fe solution. A standard–sample–standard bracketing method was used to correct for mass bias and instrument drift. Both $\delta^{56}Fe$ and $\delta^{57}Fe$ were determined relative to the international standard IRMM-014 with a 2σ uncertainty:

$$\delta^{56}Fe_{sample} = \left[\left(^{56}Fe/^{54}Fe\right)_{sample} \Big/ \left(^{56}Fe/^{54}Fe\right)_{IRMM-014} - 1\right] \times 1000\ [0/00]$$

$$\delta^{57}Fe_{sample} = \left[\left(^{57}Fe/^{54}Fe\right)_{sample} \Big/ \left(^{57}Fe/^{54}Fe\right)_{IRMM-014} - 1\right] \times 1000\ [0/00]$$

Analytical reproducibility on $\delta^{56}Fe$ and $\delta^{57}Fe$ is better than ±0.06‰ (2SD) based on repeated analyses of several international standards against an in-house stock solution G-Fe which has a $\delta^{56}Fe$ value of 0.73 ‰ on the IRMM-014 scale (Du et al., 2017; Ye et al., 2020). The measured DTS-2b and AGV-2 geological standards, which were purified and measured together with samples in this study, yield $\delta^{56}Fe$ values of $0.04 \pm 0.02$ ‰ ($n = 4$, 2SD) and $0.10 \pm 0.04$ ‰ ($n = 4$, 2SD), consistent with the recommended values (e.g., He et al., 2015).

## 4. Results

The K and Fe isotope data, together with published major and trace element and other isotope data are listed in Supplementary Table S1.

The $\delta^{41}K$ values of the studied samples range from $0.00 \pm 0.09$ ‰ to $-0.55 \pm 0.08$ ‰ (Supplemental Material 1). The $\delta^{41}K$ of the transitional and calc-alkaline samples range from $0.00 \pm 0.09$ ‰ to $-0.41 \pm 0.08$ ‰, with four samples showing heavier K isotope signatures (average $-0.11 \pm 0.06$ ‰), and the rest with an average of $-0.37 \pm 0.03$ ‰. In contrast, the shoshonitic-ultrapotassic samples exhibit a smaller variation ranging from $-0.32 \pm 0.06$ ‰ to $-0.55 \pm 0.08$ ‰ that is overall slightly lighter than the transitional to calc-alkaline samples (Fig. 3A–C).

The transitional and calc-alkaline samples have similar Fe isotope compositions, with $\delta^{56}Fe$ values ranging from $-0.06 \pm 0.07$ ‰ to $0.19 \pm$

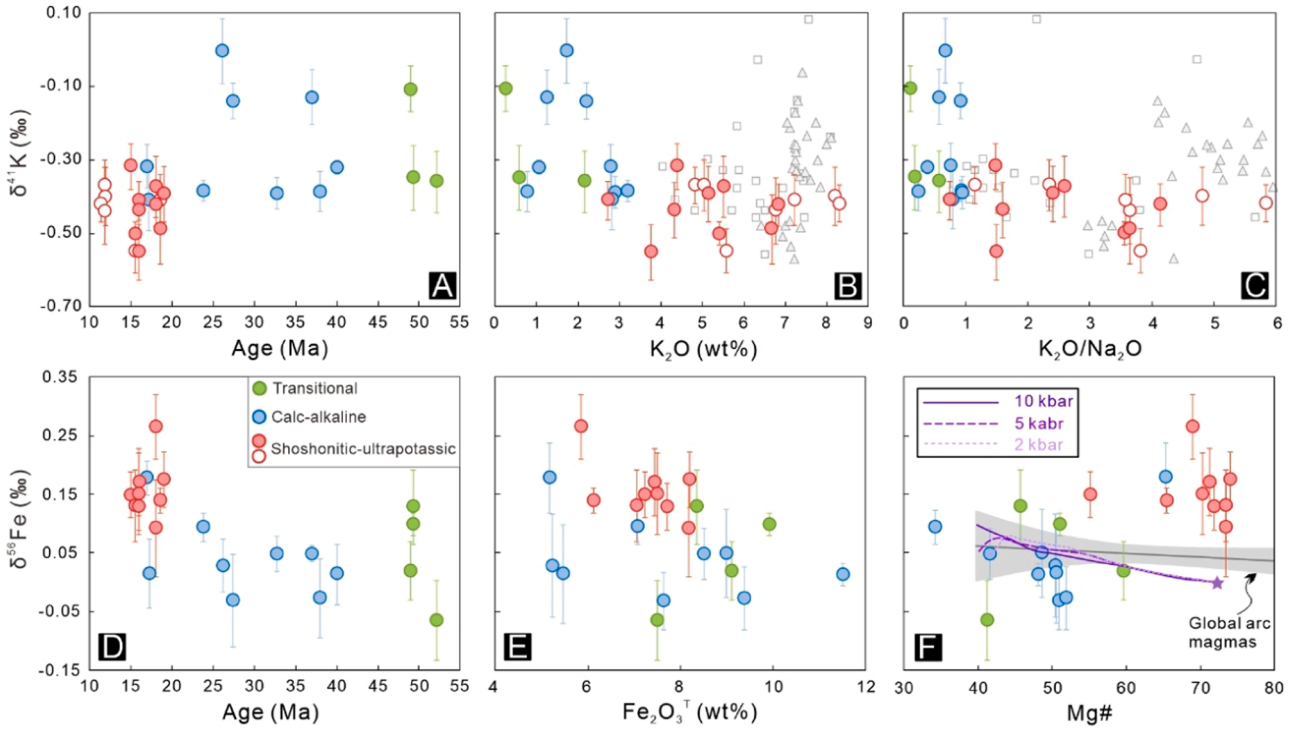


**Fig. 3.** Potassium and iron isotope compositions of the volcanic rocks from Western Anatolia. $\delta^{41}K$ as a function of (A) age (Ma), (B) $K_2O$ (wt%) and (C) $K_2O/Na_2O$. Previously published $\delta^{41}K$ values for ultrapotassic lavas from Western Anatolia (open cycles) are from Wang et al. (2021b). K isotope data of shoshonitic-ultrapotassic rocks from Qingling orogenic belt (triangle; Liu et al., 2021; Yang et al., 2023) and southeastern Tibetan Plateau (square; Miao et al., 2023) is shown in (B) and (C) for comparison. $\delta^{56}Fe$ as a function of (D) age (Ma), (E) $Fe_2O_3^T$ (wt%) and (F) Mg#. Gray shaded area in (F) represents the trend of global arc magmas (Foden et al., 2018). Purple curves in (F) are Mg#-$\delta^{56}Fe$ evolution paths under pressures from 10 kbar to 2 kbar calculated by pMELTS (see details in Supplemental Material 2).

0.04 ‰ and an average of 0.05 ± 0.07 ‰. In comparison, the $\delta^{56}Fe$ values of the shoshonitic-ultrapotassic samples vary from 0.09 ± 0.08 ‰ to 0.26 ± 0.05 ‰, with an average of 0.16 ± 0.05 ‰ (Fig. 3D).

Two samples of Proterozoic augen gneiss from the Menderes Massif were analyzed as representative of local continental crust and yielded $\delta^{41}K$ values of –0.42 ‰ and –0.45 ‰, and $\delta^{56}Fe$ values of 0.35 ‰ and 0.24 ‰.

## 5. Discussion

### *5.1. Subducted components as K sources of Western Anatolia magmas: insights from K isotopes*

The large K isotope variability in the Western Anatolia volcanic rocks may be caused by several processes, including post-eruption alteration, crystal fractionation coupled with crustal assimilation (AFC process), and source metasomatism by subducted oceanic/continental components (fluid/melts).

Post eruption low-temperature alteration results in partitioning of heavy K isotopes into the fluid phase, leading to weathered products with lower $\delta^{41}K$ values (Li et al., 2019). Although some of the shoshonitic and ultrapotassic rocks have elevated LOI values (up to 7.5 wt%; Table S1), similar to many potassic samples from Western Anatolia (e.g., Ersoy and Palmer, 2013), their chemical indices of alteration (CIA, 32–41) are in line with fresh igneous rocks (CIA < 50). Furthermore, there is no clear relationship between the $\delta^{41}K$ values and LOI or the CIA values of the entire data set or within the different types of volcanic rock (Fig. S1). Hence, there is no evidence that the range in $\delta^{41}K$ values reflects post-eruption alteration.

Potassium isotope fractionation as a result fractional crystallization is restricted to highly differentiated magma stages (e.g., $SiO_2$ > 70 wt%; Hu et al., 2021b; Huang et al., 2023). However, the Western Anatolia samples in this study have low $SiO_2$ contents (<60 wt%), and the $\delta^{41}K$ values of the samples do not correlated with the $SiO_2$ and MgO contents (Fig. S2). In addition, two gneiss samples, representative of wall rock of the shoshonitic-ultrapotassic lavas, have $\delta^{41}K$ values (–0.42 ‰ and –0.45 ‰) slightly higher than the isotopically lightest ultrapotassic samples (Fig. 3A–C), hence assimilation of these gneisses failed to generate the low-$\delta^{41}K$ signatures in shoshonitic-ultrapotassic lavas (Fig. S2). Taken together, these observations indicate the limited contribution of AFC process to the K isotope variation of the Western Anatolian lavas.

The wide variation of K isotope compositions in the Western Anatolia lavas are most likely inherited from a mantle source that was enriched in K by slab-derived components (fluids/melts). In a study of the K isotope composition of volcanic rocks from the Izu arc, Parendo et al. (2022) compared the K/Yb – Nb/Yb relationship of the Izu volcanic rocks to that in MORB (Fig. 4) and concluded that ~90 % of the K in the Izu lavas are derived fluids/melts originating from the subducted slab. Similar degrees of K-enrichment are seen in the Lesser Antilles lavas (Hu et al., 2021a) and Western Anatolia samples of this study (Fig. 4). However, while the degree of K enrichment is similar in arc lavas from the Lesser Antilles and Izu arcs, they show distinct K isotope compositions. As shown in Fig. 5, most of the Izu arc lavas lie on a mixing line between a depleted mantle (DM) endmember and one defined by fluids derived from altered oceanic crust (Parendo et al., 2022), whereas most of the Lesser Antilles data fall on a mixing line between local subducted sediments (LA sediment) and the DM endmember (Hu et al., 2020). These two trends are interpreted to reflect a dominant aqueous fluid source of K in the Izu arc and a dominant sediment melt source of K in the Lesser Antilles (Hu et al., 2021a; Parendo et al., 2022). While some of the calc-alkaline and transitional Western Anatolian lavas have elevated $\delta^{41}K$ values that may reflect an aqueous fluid source of K, the trend defined by shoshonitic-ultrapotassic samples towards low $\delta^{41}K$ and radiogenic $^{87}Sr/^{86}Sr$ signatures likely reflect incorporation of isotopically light K from subducted terrestrial sediments and/or continental

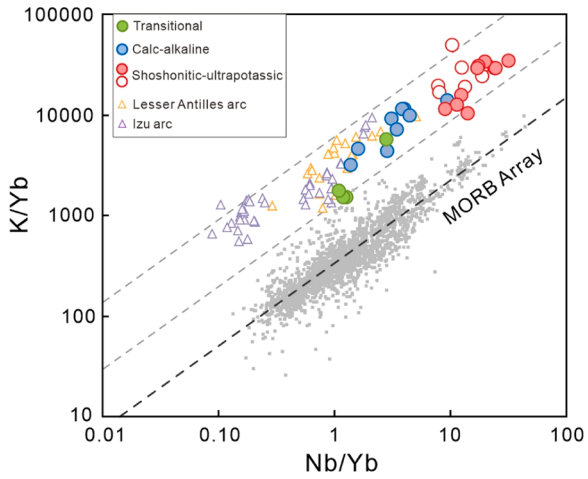


**Fig. 4.** K/Yb versus Nb/Yb for volcanic rocks from Western Anatolia, Izu arc (Parendo et al., 2022) and Lesser Antilles (Hu et al., 2021a), compared to mid-ocean ridge basalts (Gale et al., 2013).

crust (Fig. 5A). Other transitional and calc-alkaline samples with mantle-like $\delta^{41}K$ values may reflect a mixed fluid and sediment sources of K (Fig. 5).

Further insights into the origin of the K isotope signature of the Anatolian samples can be gathered by comparison with their B isotope compositions. Both B and K are fluid mobile elements during subduction zone processes, and the heavy isotopes are preferentially partitioned into the fluid phase during slab dehydration for both isotope systems (Rosner et al., 2003; Liu et al., 2020). Both elements are also incompatible during mantle melting, but their isotopes exhibit little fractionation. The preferential partitioning of the heavy B and K isotopes into the fluids dehydrated from the slab leaves residual phases, such as phengite that is a major repository for K and B in subducted materials, to have progressively lighter $\delta^{11}B$ and $\delta^{41}K$ values (Palmer et al., 2019; Liu et al., 2020; Fig. S3), as indicated by the positive correlation between $\delta^{11}B$ and $\delta^{41}K$ in HIMU-type metabasites exhumed from serpentinite mud volcanoes from the Mariana forearc (Liu et al., 2023). Therefore, the light $\delta^{11}B$ values observed in shoshonitic-ultrapotassic rocks in Western Anatolia are thought to be inherited from the metasomatized mantle modified by deeply subducted crustal material (e.g., sediments) that acquired a light B isotope signature in K-rich phases (such as phengite) (Palmer et al., 2019). However, there are no clear co-variations of $\delta^{41}K$ with metamorphic grade in metasediments from western Alps, suggesting negligible K isotope fractionation during prograde metamorphism, because dehydration was limited to the bulk-rock scale and thus limited K loss during the entire metamorphic history (Wang et al., 2022). In contrast to the study of Wang et al. (2022), the shoshonitic-ultrapotassic rocks in this study show negative $\delta^{11}B$ values (Fig. 6), reflecting the incorporation of subducted sediments that had experienced extensive dehydration as they were transported into the mantle (Palmer et al., 2019). During this process $^{41}K$ is also preferentially fractionated into the fluids. In this scenario, dehydration processes during subduction lead to a further enrichment of light K isotopes in the metamorphic products, hence magmas that incorporate phases such as phengite in their mantle sources may show lighter K isotope signatures. Indeed, the Western Anatolia shoshonitic-ultrapotassic samples lie on a trend towards low $\delta^{41}K$ and low $\delta^{11}B$ values, consistent with the incorporation of sedimental/continental phengite to their mantle sources (Fig. 6).

However, three of the calc-alkaline samples and one of the transitional samples lie on a trend towards positive $\delta^{41}K$ values and negative $\delta^{11}B$ values. This trend may reflect the observation that B appears to be driven off the subducting slab closer to the subduction zone than K. For example, within the Andean central volcanic zone, $\delta^{11}B$ and B/K ratios are highest closest to the volcanic front, where the depth to the Wadati-Benioff Zone (WBZ) is shallowest, and both values progressively decrease with increasing WBZ depth (Fig. 7) (Rosner et al., 2003). Similarly, Parendo et al. (2022) observed an across-arc $\delta^{41}K$ decrease in lavas of the Izu arc in which the arc-front lavas are isotopically heavier than the rear arc lavas by about 0.14 ‰, but to a lesser extent compared with B isotope variation within the Andean lavas (Fig. 7A). These suggest that B and thus $^{11}B$ release from subducted slab proceeds much more efficiently than K and heavy K isotopes during dehydration processes. Therefore, the inverse trend between $\delta^{11}B$ and $\delta^{41}K$ value for some of the Anatolian data (Fig. 6) may reflect eruption of these rocks at a distance from the volcanic front during the collisional phase of volcanism where the slab-derived influx of boron is declining, but the influx of K/B is increasing.

Further evidence that the high $\delta^{41}K$ samples contain a significant component of slab-derived aqueous fluids is provided by the observation that the four high-$\delta^{41}K$ samples have elevated Cs/Th ratios, consistent with the contribution of slab-derived fluids, as Cs significantly partitions into the aqueous fluid over Th during dehydration processes (Zheng,

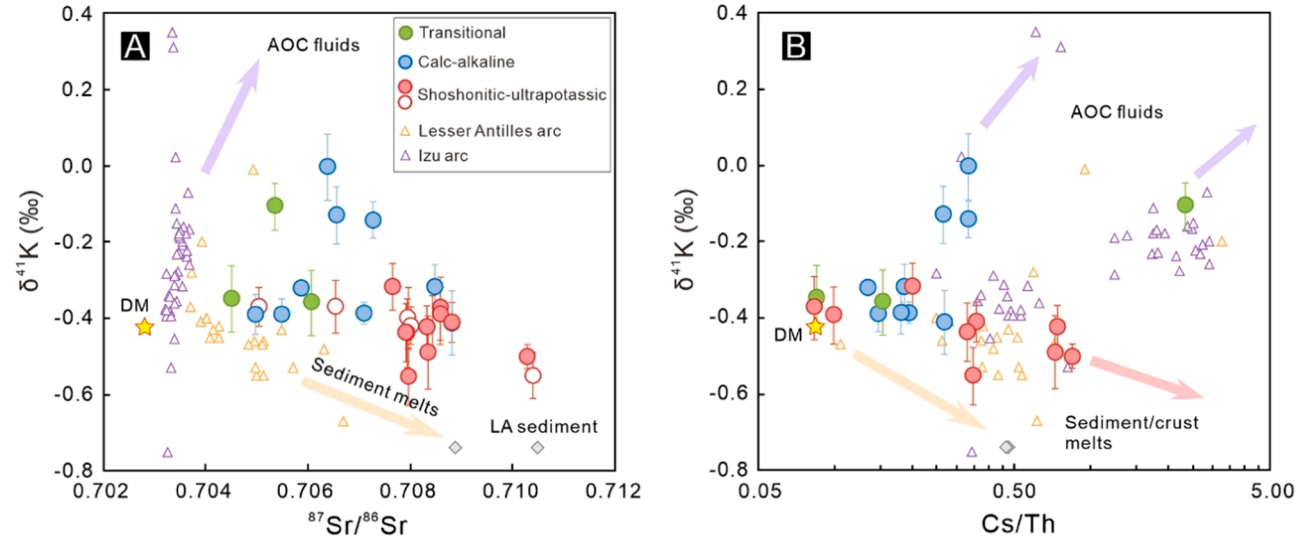


**Fig. 5.** $\delta^{41}K$ versus $^{87}Sr/^{86}Sr$ (A) and Cs/Th (B) for volcanic rocks from Western Anatolia, Izu arc (Parendo et al., 2022) and Lesser Antilles (Hu et al., 2021a). The composition of depleted mantle (DM) is shown for comparison (Hu et al., 2021b; Workman and Hart, 2005).

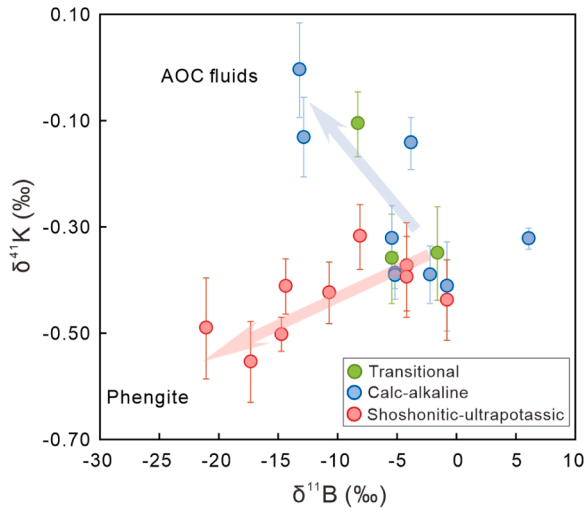


**Fig. 6.** $\delta^{41}K$ versus $\delta^{11}B$ (Palmer et al., 2019) for volcanic rocks from Western Anatolia.

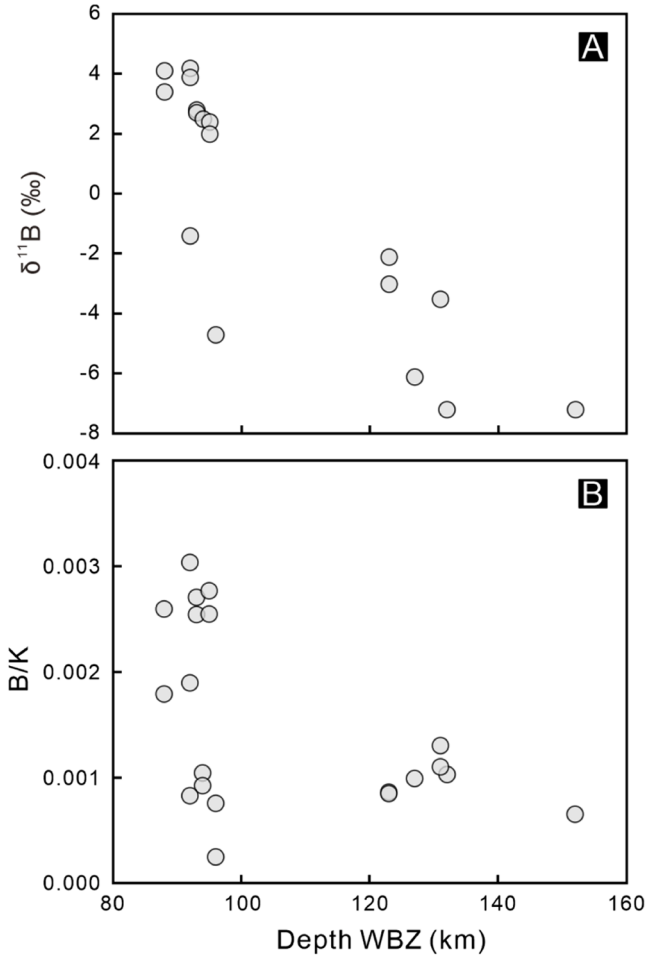


**Fig. 7.** $\delta^{11}B$ (A), B/K (B) versus depth to Wadati-Benioff Zone (WBZ) in Central Andes arc volcanic rocks (data from Rosner et al., 2003).

2019 and references therein) (Fig. 5B).

### 5.2. *Mantle modification by crustal recycling beneath Western Anatolia: insights from Fe isotopes*

It is notable that the shoshonitic-ultrapotassic lavas have heavy Fe isotope compositions compared with the transitional and calc-alkaline volcanic rocks, and with MORB ($\delta^{56}Fe = 0.105 \pm 0.006$ ‰; Teng et al., 2013) and global mafic arc magmas ($\delta^{56}Fe = 0.050 \pm 0.025$ ‰; Foden et al., 2018; Fig. 3F). There are four possible mechanism that may fractionate Fe isotopes in Western Anatolia magmas: (1) slab-derived fluid addition, (2) isotope fractionation during fractional crystallization; (3) isotope fractionation during mantle partial melting; (4) isotope variation inherited from the magma source.

Several samples from transitional and calc-alkaline volcanic suits show elevated $\delta^{41}K$ values that are related to fluid flux from the down going slab. The fluids tend to concentrate light Fe isotopes (e.g., Debret et al., 2016), and adding these fluids will drive the mantle sources and associated magmas toward lighter Fe isotope compositions. However, there are no clear co-variations of $\delta^{56}Fe$ with any fluid indicators such as Ba/La, B/La and Cs/Th (Fig. S4), indicating the negligible contribution of fluid addition on the Fe isotope variations of Western Anatolian lavas. This can be understood in the context of mass balance considering the extremely low Fe content in slab-derived fluids (~0.1 wt%; Debret et al., 2016) versus the substantial Fe reservoirs of the peridotite-dominated mantle (~8.2 wt%; Workman and Hart, 2005).

The Eocene transitional and calc-alkaline eruptive rock samples have Mg# (Mg/(Mg+Fe) × 100; molar ratio) values of 65 to 40 (Fig. 3F). These values are lower than the Mg# of global primitive arc magmas in equilibrium with mantle peridotite (65 to 75; Schmidt and Jagoutz, 2017). Thus, the transitional and calc-alkaline magmas have experienced magmatic differentiation, which may influence the $\delta^{56}Fe$ values of these samples. After a few percent of olivine fractionation, calc-alkaline basaltic magmas may saturate in clinopyroxene and then in amphibole and spinel (Nandedkar et al., 2014). Thus, it is hard to correct the effect of fractional crystallization on the Fe isotope composition of the transitional and calc-alkaline magmas. In this study, we use pMELTS (Ghiorso et al., 2002) to evaluate the effect of fractional crystallization on Fe isotope fractionation under 0.2–1.0 GPa (garnet undersaturation, as indicated by their low La/Yb ratios) and a constant oxygen fugacity of FMQ starting from a primitive basaltic composition from Western Anatolia (see more details in Supplemental Material 2). The main conclusion of this modeling is that the magnitude of Fe isotope fractionation induced by fractional crystallization cannot exceed ~0.06 ‰ as a primitive melt evolves to a Mg# of ~45 before magnetite saturation (Fig. 3F). Hence, isotope fractionation during fractional crystallization only has a limited effect on the Fe isotope compositions of the transitional and calc-alkaline eruptive rocks, and the relatively low and dispersed $\delta^{56}Fe$ values must therefore largely reflect source-related processes.

In contrast, the shoshonitic-ultrapotassic rocks have high Mg# values (65 to 74) and MgO contents (≥6 wt%), which are closer to those of a primitive melt. The Fe isotopes in the shoshonitic-ultrapotassic rocks should, therefore, be less affected by the effects of fractional crystallization during magma evolution. Thus, the elevated $\delta^{56}Fe$ values of the shoshonitic-ultrapotassic lavas and the $\delta^{56}Fe$ difference between the shoshonitic-ultrapotassic and transitional and calc-alkaline samples (Fig. 3D-F) likely reflect partial melting of distinct mantle sources.

Partial melting can produce higher $\delta^{56}Fe$ melts because $Fe^{3+}$ is more incompatible than $Fe^{2+}$ during mantle melting in which the smaller $Fe^{3+}$ sites tend to be associated with stiffer Fe-O bonds and thus enrich heavy Fe isotopes (e.g., Teng et al., 2013; Dauphas et al., 2014). Hence, extraction of $^{56}Fe$-enriched melts will drive the residues towards lighter Fe isotope compositions (e.g., Weyer and Ionov, 2007; Williams and Bizimis, 2014). The high La/Yb ratios and $\delta^{56}Fe$ values within the shoshonitic-ultrapotassic lavas are consistent with variable amounts of

garnet retention in the melt residues, which favors Yb and light Fe isotopes (Sossi and O'Neil, 2017; Ye et al., 2020). Hence, we first examine whether the La/Yb and $\delta^{56}$Fe variations in the Western Anatolia lavas could be produced by partial melting of a peridotite source under a range of pressures.

The peridotite source is assumed to have La and Yb concentrations similar to that of the depleted MORB mantle (La/Yb = 0.66; Workman and Hart, 2005). According to pMELTS modeling (Ghiorso et al., 2002) (see details in Supplemental Material 2), partial melting of lherzolite (an analog for the upper mantle) at 2–3 GPa (from spinel to garnet phase, Fig. 8A) can generate melts with La/Yb ratios similar to those of the transitional and calc-alkaline samples (2 to 18) (Fig. 8B). In addition, incorporating slab-derived fluids (as indicated by high $\delta^{41}$K values) may slightly increase La/Yb in the peridotite sources because La is more compatible than Yb in aqueous fluids (e.g., Zheng, 2019). Thus, fluid metasomatism coupled with some extent of amphibole fractionation may explain the high-La/Yb calc-alkaline samples (Fig. 8B). The Fe isotope fractionation during partial melting (defined as $\Delta^{56}Fe = \delta^{56}Fe_{melt} - \delta^{56}Fe_{initial}$) ranges from ~0.06 ‰ to ~0.03 ‰ during 2 % to 20 % melting. Superimposing this melting-induced fractionation on the lherzolite ($\delta^{56}$Fe = –0.011 ± 0.019 ‰, 2σ; Johnson et al., 2020) can generate melts with $\delta^{56}$Fe from 0.02 ‰ to 0.05 ‰ (Figs. 8C and 9A), that encompasses the average $\delta^{56}$Fe value of the transitional and calc-alkaline rocks ($\delta^{56}$Fe = 0.05 ± 0.07 ‰, 1SD, $n$ = 13), despite the fact that they show a large range in Fe isotope compositions. To explain the large $\delta^{56}$Fe dispersion, we suggest that (1) some samples with low $\delta^{56}$Fe may be derived from more depleted mantle sources that experienced more extensive melt extraction (e.g., Weyer and Ionov, 2007; Williams and Bizimis, 2014), while (2) individual samples with higher $\delta^{56}$Fe values might reflect peridotite source heterogeneity due to melt percolation (e.g., Weyer and Ionov, 2007). However, the shoshonitic-ultrapotassic lavas are characterized by high $\delta^{56}$Fe values (0.16 ± 0.05 ‰, 1SD) and La/Yb ratios (20 to 44) which cannot be reproduced by partial melting of a garnet lherzolite source.

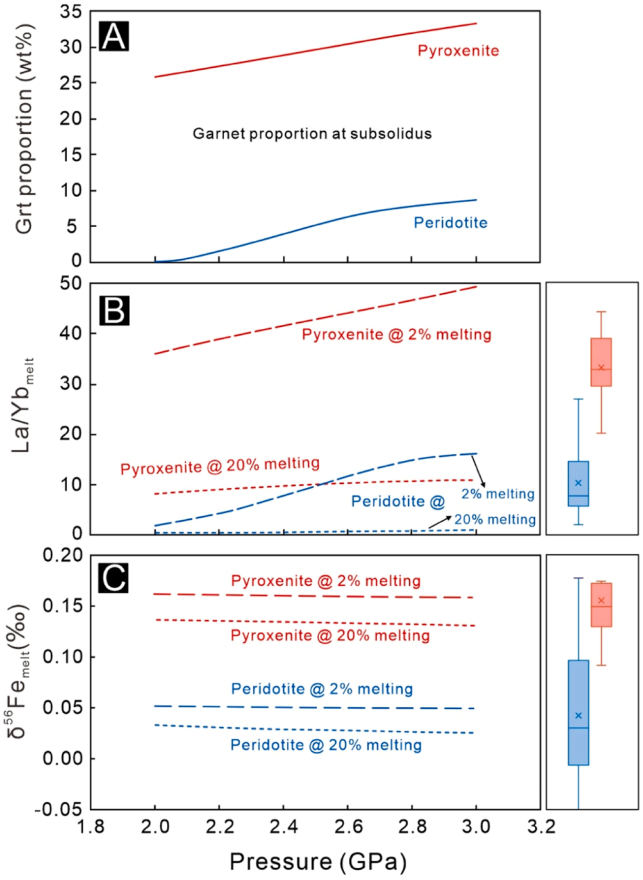


**Fig. 8.** Lithology control on La/Yb ratio and Fe isotope fractionation during batch melting. Results are based on pMELTS simulation of peridotite (KLB1) and pyroxenite (M5–40) under 2.0 to 3.0 GPa, 0 wt% $H_2O$, and a constant $fO_2$ of FMQ. (A) Garnet abundance at subsolidus. (B) Melt La/Yb ratios generated by batch melting of the peridotite and pyroxenite sources from 2 % to 20 % melting degrees, respectively. (C) Melt $\delta^{56}$Fe values generated by batch melting of the peridotite and pyroxenite from 2 % to 20 % melting degrees, respectively. The La/Yb ratios (B) and $\delta^{56}$Fe values (C) of the Western Anatolia samples are presented as box and whisker plots on the right side, in which the blue boxes represent the transitional and calc-alkaline samples and the red boxes represent the shoshonitic-ultrapotassic samples. See more modeling details in the main text and Supplemental Material 2.

It is necessary to examine whether mixing of mantle peridotites with subducted sediments can produce the high-$\delta^{56}$Fe values of shoshonitic-ultrapotassic lavas because of their sediment-like K, B and Sr isotope signatures (Figs. 5A and 6). However, the shoshonitic-ultrapotassic lavas have generally higher $\delta^{56}$Fe values than transitional and calc-alkaline lavas, and there are no clear binary mixing trends of $\delta^{56}$Fe with $^{87}Sr/^{86}Sr$, $^{143}Nd/^{144}Nd$, $\delta^{11}$B and $\delta^{41}$K (Fig. S5), indicating that the high-$\delta^{56}$Fe signatures cannot be explained by a simple mixing model.

Compared with the transitional and calc-alkaline samples, the shoshonitic-ultrapotassic samples have systematically higher La/Yb ratios, lower $Al_2O_3$ contents, and elevated $\delta^{56}$Fe signatures (Fig. 9), consistent with greater garnet retention in their sources. These observations imply that the sources of the shoshonitic-ultrapotassic and calc-alkaline lavas have different chemical compositions and mineral assemblages. Williams and Bizimis (2014) noted that pyroxenites have systematically higher $\delta^{56}$Fe values than peridotites, and could thus serve as the source of some high-$\delta^{56}$Fe basalts, e.g., ocean island basalts (OIBs; e.g., Konter et al., 2016; Wang et al., 2021a). Furthermore, olivine phenocrysts from Western Anatolia ultrapotassic lavas have higher Ni and low CaO contents for a given Mg# than those in MORBs (Prelević and Foley, 2007; Prelević et al., 2012; Foley et al., 2013), similar to the secondary pyroxenites produced by the reaction between slab-derived melt and peridotite (Sobolev et al., 2007), because the $D_{Ni}$ (mineral-melt partition coefficient for Ni) is much lower for pyroxenites than olivine. Thus, a pyroxenite source can release more Ni into the melt than a peridotite source (e.g., Sobolev et al., 2005). This inference is also consistent with the observation that the majority of ultrapotassic rocks from Western Anatolia contain high-forsterite olivine xenocrysts containing Cr-rich spinel inclusions, suggesting an ultra-depleted peridotite source (Prelević and Foley, 2007); while their whole rocks are isotopically akin to the crust-derived sedimentary materials (lower $\delta^{41}$K values in this study; radiogenic $^{87}Sr/^{86}Sr$ and $^{207}Pb/^{204}Pb$ ratios, and unradiogenic $^{143}Nd/^{144}Nd$ and $^{176}Hf/^{177}Hf$ ratios; e.g., Prelević et al., 2012; Ersoy and Palmer, 2013). Thus, the interaction of crust-derived melts with the ultra-depleted mantle resulted in the production of pyroxenite-rich veins/domains at the expense of olivine (Prelević et al., 2012, 2013). The crust-derived melts, e.g., granites and leucosomes, commonly have $\delta^{56}$Fe values of ≥0.1 ‰ (e.g., Foden et al., 2015; Xu et al., 2017b) that are systematically higher than those of peridotites ($\delta^{56}$Fe ~0 ‰; Johnson et al., 2020). Thus, such a process is expected to cause further enrichment of heavy Fe isotopes in the pyroxenite-rich veins/domains by Fe-Mg inter-diffusion as observed in the garnet pyroxenites from Hannuoba, North China Craton (Zhao et al., 2017) and the lherzolites from Purang ophiolite, southwestern Tibet (Su et al., 2015), and reviewed by Johnson et al. (2020).

To further test this hypothesis, we used pMELTS (Ghiorso et al., 2002) to simulate the partial melting of a garnet pyroxenite (M5–40, close to the average composition of pyroxenites; Lambart et al., 2009) at pressures of 2 to 3 GPa (see details in Supplemental Material 2). As shown by Fig. 8A, the pyroxenite source has higher garnet proportions (from 25 % to 33 %) at subsolidus temperatures than a peridotite source at a given pressure. Although pyroxenites show a large dispersion in La/Yb ratios (~0.01 to 19; e.g., Gysi et al., 2011; France et al., 2015), the

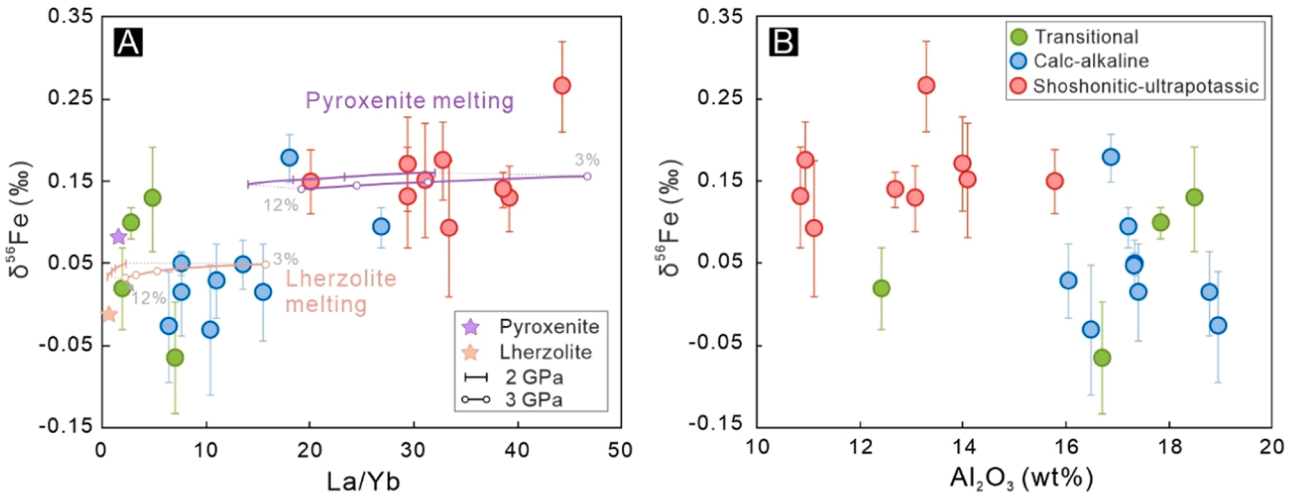


**Fig. 9.** Fe isotope composition of the Western Anatolian lavas as a function of (A) La/Yb and (B) $Al_2O_3$ (wt%). Solid lines in (A) show the Fe isotope compositions of lherzolite- and pyroxenite-derived melts under pressures of 2.0 to 3.0 GPa modeled by pMELTS (see more details in main text and Supplemental Material 2), at melt fractions given in grey.

interaction between the crustal/sedimental melts and peridotites tend to drive light REE enrichment in the resultant pyroxenites (e.g., Gysi et al., 2011) because the melts favor light REE over heavy REE (Wang and Foley, 2018). In this scenario, the pyroxenite in the modeling is assumed to have slight La enrichment relative to Yb, similar to the garnet pyroxenite from the French Massif Central (La/Yb = 1.56; France et al., 2015). As shown in Fig. 8B, partial melting of a garnet-rich pyroxenite source can produce melts with La/Yb ratios similar to those observed in the shoshonitic-ultrapotassic lavas (20 to 44). The melting-induced Fe isotope fractionation ($\Delta^{56}Fe = \delta^{56}Fe_{melt} - \delta^{56}Fe_{initial}$) ranges from 0.08 ‰ to 0.05 ‰ at 2 % to 20 % melting, which is slightly higher than those of the peridotite source due to more extensive garnet retention in their sources. Superimposing the melting fractionation onto the initial pyroxenite $\delta^{56}Fe$ of 0.083 ‰ (Johnson et al., 2020) can reproduce isotopically heavy melts that encompass most of the $\delta^{56}Fe$ values observed in the shoshonitic-ultrapotassic lavas (Figs. 8C and 9A).

Overall, therefore, the transitional and calc-alkaline eruptive rocks with arc magma-like $\delta^{56}Fe$ signatures can be reproduced by partial melting of peridotitic sources (similar to global arc magmas; Fig. 3F), whereas the shoshonitic-ultrapotassic eruptive rocks are characterized by elevated $\delta^{56}Fe$ values and La/Yb ratios that require a pyroxenite source. These results highlight that the geochemical transition from calc-alkaline to shoshonitic-ultrapotassic affinities reflect melting of a lithologically distinct lithospheric mantle (e.g., Ersoy and Palmer, 2013; Palmer et al., 2019) below Western Anatolia.

### 5.3. *Implications for the petrogenesis of ultrapotassic magmas and geochemical transition in Western Anatolia orogenic belt*

The $\delta^{41}K$ data, in conjunction with other geochemical indices (particularly $\delta^{11}B$), indicate that the ultrapotassic volcanic rocks incorporate the products of the breakdown of deeply subducted phengite during continental subduction. At high pressure (~2.4 to 5.0 GPa), phengite is the dominant repository for K in the subducted sediments,

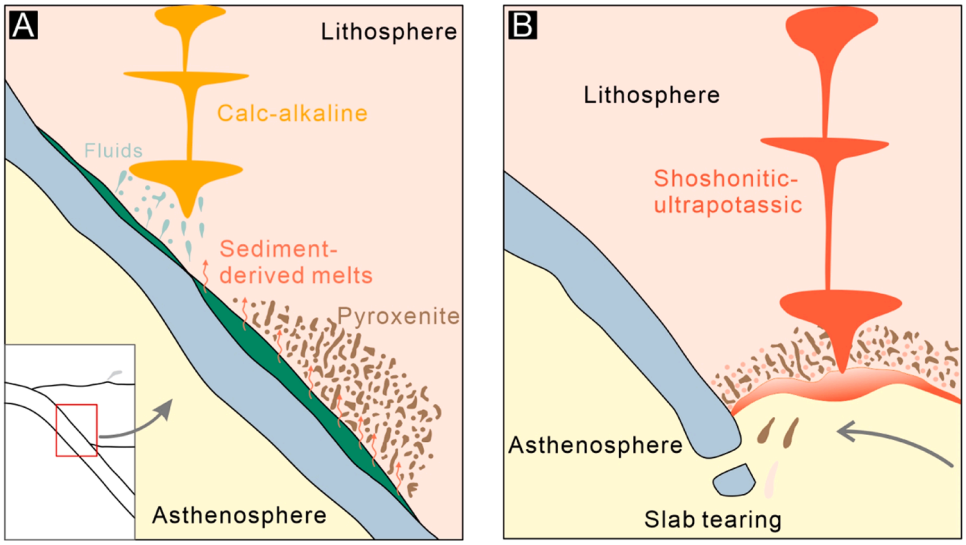


**Fig. 10.** Petrogenic model for the post-collisional, shoshonitic-ultrapotassic volcanism in Western Anatolia. (A) Eocene to early Oligocene: Continuing convergence between Pontides and Anatolide-Tauride resulted in the deep subduction of sediment and continental crustal slices into the mantle. The mantle peridotite beneath the collision zone was intensively metasomatized by the sediment-derived melts, forming the veins/domains of $K_2O$-enriched pyroxenite. (B) Late Oligocene to Middle Miocene: the slab tearing/slab roll-back beneath the Western Anatolia triggered the asthenosphere upwelling. This process resulted in partial melting of the previously metasomatized pyroxenites, generating the shoshonitic-ultrapotassic magmas.

and thus its breakdown results in potassic melt, in which the $K_2O/Na_2O$ of the melts increase with increasing pressure (e.g., Schmidt et al., 2004; Schmidt, 2015). Thus, breakdown of phengite could lead to metasomatism of the overlying mantle and formation of K-enriched mantle mineral phases such as phlogopite (e.g., Schmidt, 2015; Prelević et al., 2012).

The $\delta^{56}$Fe data further indicate that the ultrapotassic volcanic rocks are derived from a predominantly pyroxenitic source, that likely formed by the interaction between peridotite and sediment-derived melt (Fig. 10A). The absence of these $\delta^{41}$K and $\delta^{56}$Fe pyroxenite signatures in the calc-alkaline and transitional rocks, suggests that the pyroxenite veins/domains were not present in the mantle beneath Western Anatolia prior to eruption of the ultrapotassic volcanics. Palmer et al. (2019) noted that the timing of onset of eruption of the ultrapotassic rocks (~19 Ma) coincided with slab rollback and/or tearing imaged by mantle tomographic studies (e.g., van Hinsbergen et al., 2010). Notably, the duration of ultrapotassic magmatism was only ~5 Myr, with Na-alkaline volcanics erupted after 12 Ma (Ersoy and Palmer, 2013).

The rapid onset and short duration of the period of ultrapotassic volcanism suggest that the K-rich metasomatism of the mantle was not pervasive, but rather confined to a network of phlogopite-pyroxenite veins within a predominantly peridotitic mantle (Prelević et al., 2012). The trigger for the breakdown of the low $\delta^{11}$B and low $\delta^{41}$K phengite may either have been rapid heating of the descending slab during rollback leading to destabilization of these phases (e.g., Stern, 2002) or detachment of the low density subducted continental crust during slab rollback (as suggested by van Hinsbergen et al., 2010). In either case, once breakdown of the phengite had resulted in the formation of the phlogopite-pyroxenite veins in the overlying mantle, the low solidus temperatures of these assemblages (Schmidt, 2015), would have led to their rapid melting during the influx of hot asthenospheric mantle during slab rollback (Fig. 10B), with ultrapotassic volcanism ceasing once the phlogopite-pyroxenite veins had been consumed.

## 6. Conclusions

(1) Transitional and calc-alkaline volcanic rocks were erupted in Western Anatolia during syn- to post-collisional stages in the region. These rocks have $\delta^{41}$K values that reflect variable contributions of slab-derived fluids to the mantle in an Andean-type continental arc setting. However, the shoshonitic-ultrapotassic volcanics that were erupted in the post-collisional stage of orogeny tend to have lower $\delta^{41}$K values that are correlated with light $\delta^{11}$B values, indicating incorporating K derived from melting of deeply subducted continental sediment and/or crust.
(2) The transitional and calc-alkaline lavas also have arc-like $\delta^{56}$Fe values that are consistent with peridotite sources, while the shoshonitic-ultrapotassic magmas have Fe isotope ratios that reflect an isotopically heavy pyroxenite source.
(3) The rapid onset and short duration (~5 Myr) of the light $\delta^{41}$K and heavy $\delta^{56}$Fe signature in the shoshonitic-ultrapotassic volcanic rocks is most consistent with the generation of phlogopite-pyroxenite veins in the sub-continental peridotitic mantle during breakdown of deeply subducted phengite during slab rollback. These veins were then melted and quickly consumed during upwelling of hot asthenospheric mantle to form the shoshonitic-ultrapotassic volcanic rocks.

## CRediT authorship contribution statement

**De-Hong Du:** Writing – original draft, Visualization, Investigation, Formal analysis. **Xiang-Long Luo:** Formal analysis. **Xiao-Lei Wang:** Writing – review & editing, Supervision, Resources, Investigation. **Martin R. Palmer:** Writing – review & editing, Validation, Resources. **E. Yalçın Ersoy:** Resources, Investigation. **Weiqiang Li:** Writing – review & editing, Supervision, Methodology, Investigation, Funding acquisition, Conceptualization.

## Declaration of competing interest

The authors declare that they have no known competing financial interests or personal relationships that could have appeared to influence the work reported in this paper.

## Data availability

Data will be made available on request.

## Acknowledgments

This work was financially supported by National Science Foundation of China (42025202 to XLW and 41873004 to WL), TÜBİTAK-CAYDAG-112Y128 to EYE, and NERC grant NE/V00736X/1 to MRP. We thank Dr. Shichao An for assistance in Fe and K isotope measurements. We thank Stefan Weyer, Haiyang Liu, and two anonymous reviewers for their constructive comments and editor Rosemary Hickey-Vargas for her efficient handling of this manuscript.

## Supplementary materials

Supplementary material associated with this article can be found, in the online version, at doi:10.1016/j.epsl.2024.118642.

## References

An, S., Luo, X., Li, W., 2022. Precise measurement of $^{41}K/^{39}K$ ratios by high-resolution multicollector inductively coupled plasma mass spectrometry under a dry and hot plasma setting. Rapid Commun. in Mass Sp. 36, e9289.
Condamine, P., Médard, E., Devidal, J.L., 2016. Experimental melting of phlogopite-peridotite in the garnet stability field. Contrib. Mineral. Petrol. 171, 1–26.
Dauphas, N., Roskosz, M., Alp, E.E., Neuville, D.R., Hu, M.Y., Sio, C.K., Tissot, F.L.H., Zhao, J., Tissandier, L., Medard, E., Cordier, C., 2014. Magma redox and structural controls on iron isotope variations in Earth's mantle and crust. Earth Planet. Sci. Lett. 398, 127–140.
Debret, B., Millet, M.A., Pons, M.L., Bouilhol, P., Inglis, E., Williams, H., 2016. Isotopic evidence for iron mobility during subduction. Geology 44, 215–218.
Du, D.H., Wang, X.L., Yang, T., Chen, X., Li, J.Y., Li, W., 2017. Origin of heavy Fe isotope compositions in high-silica igneous rocks: a rhyolite perspective. Geochim. Cosmochim. Acta 218, 58–72.
Erkül, S.T., Erkül, F., 2012. Magma interaction processes in syn-extensional granitoids: the Tertiary Menderes Metamorphic Core Complex, western Turkey. Lithos 142, 16–33.
Ersoy, E.Y., Palmer, M.R., 2013. Eocene-Quaternary magmatic activity in the Aegean: implications for mantle metasomatism and magma genesis in an evolving orogeny. Lithos 180, 5–24.
Foden, J., Sossi, P.A., Nebel, O., 2018. Controls on the iron isotopic composition of global arc magmas. Earth Planet. Sci. Lett. 494, 190–201.
Foden, J., Sossi, P.A., Wawryk, C.M., 2015. Fe isotopes and the contrasting petrogenesis of A-, I-and S-type granite. Lithos 212, 32–44.
Foley, S.F., Prelevic, D., Rehfeldt, T., Jacob, D.E., 2013. Minor and trace elements in olivines as probes into early igneous and mantle melting processes. Earth Planet. Sci. Lett. 363, 181–191.
Foley, S., Venturelli, G., Green, D.H., Toscani, L., 1987. The ultrapotassic rocks: characteristics, classification, and constraints for petrogenetic models. Earth-Sci. Rev. 24, 81–134.
France, L., Chazot, G., Kornprobst, J., Dallai, L., Vannucci, R., Grégoire, M., Boivin, P., 2015. Mantle refertilization and magmatism in old orogenic regions: the role of late-orogenic pyroxenites. Lithos 232, 49–75.
Gale, A., Dalton, C.A., Langmuir, C.H., Su, Y., Schilling, J.G., 2013. The mean composition of ocean ridge basalts. Geochem. Geophy. Geosy. 14, 489–518.
Ghiorso, M.S., Hirschmann, M.M., Reiners, P.W., Kress III, V.C., 2002. The pMELTS: a revision of MELTS for improved calculation of phase relations and major element partitioning related to partial melting of the mantle to 3GPa. Geochem. Geophy. Geosy. 3, 1–35.
Guo, Z., Wilson, M., Zhang, M., Cheng, Z., Zhang, L., 2015. Post-collisional ultrapotassic mafic magmatism in South Tibet: products of partial melting of pyroxenite in the mantle wedge induced by roll-back and delamination of the subducted Indian continental lithosphere slab. J. Petrol. 56, 1365–1406.
Gysi, A.P., Jagoutz, O., Schmidt, M.W., Targuisti, K., 2011. Petrogenesis of pyroxenites and melt infiltrations in the ultramafic complex of Beni Bousera, northern Morocco. J. Petrol. 52, 1679–1735.

He, Y., Ke, S., Teng, F.Z., Wang, T., Wu, H., Lu, Y., Li, S., 2015. High-precision iron isotope analysis of geological reference materials by high-resolution MC-ICP-MS. Geostand. Geoanal. Res. 39, 341–356.
Hirschmann, M.M., Kogiso, T., Baker, M.B., Stolper, E.M., 2003. Alkalic magmas generated by partial melting of garnet pyroxenite. Geology 31, 481–484.
Hu, Y., Teng, F.Z., Chauvel, C., 2021a. Potassium isotopic evidence for sedimentary input to the mantle source of Lesser Antilles lavas. Geochim. Cosmochim. Acta 295, 98–111.
Hu, Y., Teng, F.Z., Helz, R.T., Chauvel, C., 2021b. Potassium isotope fractionation during magmatic differentiation and the composition of the mantle. J. Geophys. Res. 126, e2020JB021543.
Hu, Y., Teng, F.Z., Plank, T., Chauvel, C., 2020. Potassium isotopic heterogeneity in subducting oceanic plates. Sci. Adv. 6, eabb2472.
Huang, T.Y., Teng, F.Z., Wang, Z.Z., He, Y.S., Liu, Z.C., Wu, F.Y., 2023. Potassium isotope fractionation during granitic magmatic differentiation: mineral-pair perspectives. Geochim. Cosmochim. Acta 343, 196–211.
Johnson, C., Beard, B., Weyer, S., 2020. High-temperature Fe isotope geochemistry. In: Johnson, C., Beard, B., Weyer, S. (Eds.), Iron Geochemistry: An Isotopic Perspective. Springer, Cham, pp. 85–147.
Konter, J.G., Pietruszka, A.J., Hanan, B.B., Finlayson, V.A., Craddock, P.R., Jackson, M. G., Dauphas, N., 2016. Unusual $\delta^{56}$Fe values in Samoan rejuvenated lavas generated in the mantle. Earth Planet. Sci. Lett. 450, 221–232.
Ku, Y., Jacobsen, S.B., 2020. Potassium isotope anomalies in meteorites inherited from the protosolar molecular cloud. Sci. Adv. 6, eabd0511.
Lambart, S., Laporte, D., Schiano, P., 2009. An experimental study of pyroxenite partial melts at 1 and 1.5 GPa: implications for the major-element composition of Mid-Ocean Ridge Basalts. Earth Planet. Sci. Lett. 288, 335–347.
Li, S., Li, W., Beard, B.L., Raymo, M.E., Wang, X., Chen, Y., Chen, J., 2019. K isotopes as a tracer for continental weathering and geological K cycling. Proc. Natl. Acad. Sci. 116, 8740–8745.
Li, W., Beard, B.L., Li, S., 2016. Precise measurement of stable potassium isotope ratios using a single focusing collision cell multi-collector ICP-MS. J. Anal. Atom. Spectrom. 31, 1023–1029.
Liu, H., Wang, K., Sun, W.D., Xiao, Y., Xue, Y.Y., Tuller-Ross, B., 2020. Extremely light K in subducted low-T altered oceanic crust: implications for K recycling in subduction zone. Geochim. Cosmochim. Acta 277, 206–223.
Liu, H., Xue, Y.Y., Wang, K., Sun, W.D., 2021. Contributions of slab-derived fluids to ultrapotassic rocks indicated by K isotopes. Lithos 396, 106202.
Liu, H., Yang, T., Xue, Y.Y., Deng, J., Xiao, Y., Sun, H., Tong, F., Wang, K., Gao, Y., Lin, K. Y., Zhang, F., Jin, X., Sun, W.D., 2023. Slab dehydration and potassium-lithium recycling in the forearc indicated by potassium and lithium isotope compositions of exhumed metabasites. Geochim. Cosmochim. Acta 360, 16–35.
Macris, C.A., Manning, C.E., Young, E.D., 2015. Crystal chemical constraints on inter-mineral Fe isotope fractionation and implications for Fe isotope disequilibrium in San Carlos mantle xenoliths. Geochim. Cosmochim. Acta 154, 168–185.
Mallik, A., Nelson, J., Dasgupta, R., 2015. Partial melting of fertile peridotite fluxed by hydrous rhyolitic melt at 2–3 GPa: implications for mantle wedge hybridization by sediment melt and generation of ultrapotassic magmas in convergent margins. Contrib. Mineral. Petrol. 169, 1–24.
Miao, Z., Li, X., Zhao, Z., Niu, Y., Xu, B., Lei, H., Wu, J., Yang, Y., Ma, Q., Liu, D., Wang, Q., Zhu, D.-C., Mo, X., 2023. Deciphering mantle heterogeneity associated with ancient subduction-related metasomatism: insights from Mg-K isotopes in potassic alkaline rocks. Geochim. Cosmochim. Acta 348, 258–277.
Moix, P., Beccaletto, L., Kozur, H.W., Hochard, C., Rosselet, F., Stampfli, G.M., 2008. A new classification of the Turkish terranes and sutures and its implication for the paleotectonic history of the region. Tectonophysics 451, 7–39.
Moynier, F., Hu, Y., Wang, K., Zhao, Y., Gérard, Y., Deng, Z., Moureau, J., Li, W., Simon, J.I., Teng, F.Z., 2021. Potassium isotopic composition of various samples using a dual-path collision cell-capable multiple-collector inductively coupled plasma mass spectrometer, Nu instruments Sapphire. Chem. Geol. 571, 120144.
Nandedkar, R.H., Ulmer, P., Müntener, O., 2014. Fractional crystallization of primitive, hydrous arc magmas: an experimental study at 0.7GPa. Contrib. Mineral. Petrol. 167, 1015.
Palmer, M.R., Ersoy, E.Y., Akal, C., Uysal, A.I., Genç, Ş.C., Banks, L.A., Cooper, M.J., Milton, J.A., Zhao, K.D., 2019. A short, sharp pulse of potassium-rich volcanism during continental collision and subduction. Geology 47, 1079–1082.
Parendo, C.A., Jacobsen, S.B., Kimura, J.I., Taylor, R.N., 2022. Across-arc variations in K-isotope ratios in lavas of the Izu arc: evidence for progressive depletion of the slab in K and similarly mobile elements. Earth Planet. Sci. Lett. 578, 117291.
Pourteau, A., Oberhänsli, R., Candan, O., Barrier, E., Vrielynck, B., 2016. Neotethyan closure history of western Anatolia: a geodynamic discussion. Int. J. Earth Sci. 105, 203–224.
Prelević, D., Foley, S.F., 2007. Accretion of arc-oceanic lithospheric mantle in the Mediterranean: evidence from extremely high-Mg olivines and Cr-rich spinel inclusions in lamproites. Earth Planet. Sci. Lett. 256, 120–135.
Prelević, D., Akal, C., Foley, S.F., Romer, R.L., Stracke, A., Van Den Bogaard, P., 2012. Ultrapotassic mafic rocks as geochemical proxies for post-collisional dynamics of orogenic lithospheric mantle: the case of southwestern Anatolia, Turkey. J. Petrol. 53, 1019–1055.
Prelević, D., Jacob, D.E., Foley, S.F., 2013. Recycling plus: a new recipe for the formation of Alpine–Himalayan orogenic mantle lithosphere. Earth Planet. Sci. Lett. 362, 187–197.
Rosner, M., Erzinger, J., Franz, G., Trumbull, R.B., 2003. Slab-derived boron isotope signatures in arc volcanic rocks from the Central Andes and evidence for boron isotope fractionation during progressive slab dehydration. Geochem. Geophy. Geosy. 4, 9005.
Schmidt, M.W., 2015. Melting of pelitic sediments at subarc depths: 2. Melt chemistry, viscosities and a parameterization of melt composition. Chem. Geol. 404, 168–182.
Schmidt, M.W., Jagoutz, O., 2017. The global systematics of primitive arc melts. Geochem. Geophy. Geosy. 18, 2817–2854.
Schmidt, M.W., Vielzeuf, D., Auzanneau, E., 2004. Melting and dissolution of subducting crust at high pressures: the key role of white mica. Earth Planet. Sci. Lett. 228, 65–84.
Sobolev, A.V., Hofmann, A.W., Kuzmin, D.V., Yaxley, G.M., Arndt, N.T., Chung, S.L., Danyushevsky, L.V., Elliott, T., Frey, F.A., Garcia, M.O., Gurenko, A.A., Kamenetsky, V.S., Kerr, A.C., Krivolutskaya, N.A., Matvienkov, V.V., Nikogosian, I. K., Rocholl, A., Sigurdsson, I.A., Sushchevskaya, N.M., Teklay, M., 2007. The amount of recycled crust in sources of mantle-derived melts. Science 316, 412–417.
Sobolev, A.V., Hofmann, A.W., Sobolev, S.V., Nikogosian, I.K., 2005. An olivine-free mantle source of Hawaiian shield basalts. Nature 434, 590–597.
Sossi, P.A., O'Neill, H.S.C., 2017. The effect of bonding environment on iron isotope fractionation between minerals at high temperature. Geochim. Cosmochim. Acta 196, 121–143.
Stern, R.J., 2002. Subduction zones. Rev. Geophys. 40, 1012.
Su, B.X., Teng, F.Z., Hu, Y., Shi, R.D., Zhou, M.F., Zhu, B., Liu, F., Gong, X.H., Huang, Q. S., Xiao, Y., Chen, C., He, Y.S., 2015. Iron and magnesium isotope fractionation in oceanic lithosphere and sub-arc mantle: perspectives from ophiolites. Earth Planet. Sci. Lett. 430, 523–532.
Teng, F.Z., Dauphas, N., Huang, S., Marty, B., 2013. Iron isotopic systematics of oceanic basalts. Geochim. Cosmochim. Acta 107, 12–26.
Tommasini, S., Avanzinelli, R., Conticelli, S., 2011. The Th/La and Sm/La conundrum of the Tethyan realm lamproites. Earth Planet. Sci. Lett. 301, 469–478.
Tuller-Ross, B., Savage, P.S., Chen, H., Wang, K., 2019. Potassium isotope fractionation during magmatic differentiation of basalt to rhyolite. Chem. Geol. 525, 37–45.
Van Hinsbergen, D.J.J., Kaymakci, N., Spakman, W., Torvik, T.H., 2010. Reconciling the geological history of western Turkey with plate circuits and mantle tomography. Earth Planet. Sci. Lett. 297, 674–686.
Wang, K., Jacobsen, S.B., 2016. Potassium isotopic evidence for a high-energy giant impact origin of the Moon. Nature 538, 487–490.
Wang, X.J., Chen, L.H., Hanyu, T., Shi, J.H., Zhong, Y., Kawabata, H., Miyazaki, T., Hirahara, Y., Takahashi, T., Senda, R., Chang, Q., Vaglarov, B.S., Kimura, J.I., 2021a. Linking chemical heterogeneity to lithological heterogeneity of the samoan mantle plume with Fe-Sr-Nd-Pb isotopes. J. Geophys. Res. 126, e2021JB022887.
Wang, Y., Foley, S.F., 2018. Hybridization melting between continent-derived sediment and depleted peridotite in subduction zones. J. Geophys. Res. 123, 3414–3429.
Wang, Z.Z., Teng, F.Z., Busigny, V., Liu, S.A., 2022. Evidence from HP/UHP metasediments for recycling of isotopically heterogeneous potassium into the mantle. Am. Mineral. 107, 350–356.
Wang, Z.Z., Teng, F.Z., Prelevic, D., Liu, S.A., Zhao, Z., 2021b. Potassium isotope evidence for sediment recycling into the orogenic lithospheric mantle. Geochem. Perspect. Lett. 18, 43–47.
Weyer, S., Ionov, D.A., 2007. Partial melting and melt percolation in the mantle: the message from Fe isotopes. Earth Planet. Sci. Lett. 259, 119–133.
Williams, H.M., Bizimis, M., 2014. Iron isotope tracing of mantle heterogeneity within the source regions of oceanic basalts. Earth Planet Sci. Lett. 404, 396–407.
Workman, R.K., Hart, S.R., 2005. Major and trace element composition of the depleted MORB mantle (DMM). Earth Planet. Sci. Lett. 231, 53–72.
Xu, B., Griffin, W.L., Xiong, Q., Hou, Z.Q., O'Reilly, S.Y., Guo, Z., Pearson, N.J., Gréau, Y., Yang, Z.M., Zheng, Y.C., 2017a. Ultrapotassic rocks and xenoliths from South Tibet: contrasting styles of interaction between lithospheric mantle and asthenosphere during continental collision. Geology 45, 51–54.
Xu, L.J., He, Y., Wang, S.J., Wu, H., Li, S., 2017b. Iron isotope fractionation during crustal anatexis: constraints from migmatites from the Dabie orogen, Central China. Lithos 284, 171–179.
Yang, T., Liu, H., Li, Y., Xue, Y.Y., Li, X., Wang, K., Sun, W.D., 2023. High-temperature inter-mineral potassium isotope fractionation in ultrapotassic and granitic rocks: implications for the potassium isotopic compositions of arc magmas. Chem. Geol. 641, 121770.
Ye, H., Wu, C., Brzozowski, M.J., Yang, T., Zha, X., Zhao, S., Gao, B.F., Li, W., 2020. Calibrating equilibrium Fe isotope fractionation factors between magnetite, garnet, amphibole, and biotite. Geochim. Cosmochim. Acta 271, 78–95.
Zhao, X.M., Cao, H.H., Mi, X., Evans, N.J., Qi, Y.H., Huang, F., Zhang, H.F., 2017. Combined iron and magnesium isotope geochemistry of pyroxenite xenoliths from Hannuoba, North China Craton: implications for mantle metasomatism. Contrib. Mineral. Petrol. 172, 1–26.
Zheng, Y.F., 2019. Subduction zone geochemistry. Geosci. Front. 10, 1223–1254.